INTERNATIONAL JOURNAL OF NUMERICAL MODELLING: ELECTRONIC NETWORKS, DEVICES AND FIELDS
Int. J. Numer. Model. (2013)
Published online in Wiley Online Library (wileyonlinelibrary.com). DOI: 10.1002/jnm.1931

A dynamical energy-based hysteresis model for iron loss calculation in laminated cores

S. Steentjes[1,*,†], F. Henrotte[2], C. Geuzaine[3] and K. Hameyer[1]

[1]*Institute of Electrical Machines (IEM), RWTH Aachen University, Schinkelstr. 4, D-52056 Aachen, Germany*
[2]*IMMc, Université Catholique de Louvain, Av. G. Lemaitre, B-1348 Louvain-la-Neuve, Belgium*
[3]*Department of Electrical Engineering and Computer Science, Université de Liège, Grande Traverse 10, B-4000 Liège, Belgium*

SUMMARY

This paper proposes a macroscopic model for ferromagnetic hysteresis that is well-suited for finite element implementation. The model relies on a consistent thermodynamic formulation. The stored magnetic energy and the dissipated energy are known at all times and not solely after the completion of closed hysteresis loops as is usually the case. Copyright © 2013 John Wiley & Sons, Ltd.

Received 10 May 2013; Revised 16 July 2013; Accepted 3 August 2013

KEY WORDS: hysteresis; ferromagnetism; homogenization; eddy currents; losses

1. INTRODUCTION

In a ferromagnetic sample subjected to a time varying applied magnetic field $\boldsymbol{h}(t)$, several mechanisms are responsible for the apparition of induced currents at different levels of the microstructure. In particular, two geometrical scales should be distinguished. Currents directly induced by the variation of the external magnetic field are called eddy currents. They depend on the geometry of the sample and on the rate of variation $\partial_t \boldsymbol{h}(t)$ of the applied field. On the other hand, microscopic currents are also induced locally because of the broken (jerky) motion of Bloch walls (Barkhausen effect). The dynamics of this motion is ruled by certain features of the microstructure, and it determines the intensity and the distribution of the microscopic currents, whose associated Joule losses are conventionnally called hysteresis losses. Hysteresis losses density does not depend on the geometry of the sample, neither on the frequency of the applied magnetic field (hysteresis is a quasi-static phenomenon), but it depends on the local maxima attained by the field $\boldsymbol{h}(t)$ all through the magnetization history of the sample.

The term iron losses covers the sum of these two intertwined phenomena. Conventional hysteresis models such as Preisach or Jiles–Atherton [1–3], however, address one (hysteresis) independently of the other (eddy currents). On the contrary, we present in this paper a strongly coupled model that addresses both phenomena simultaneously so that the interplay between skin effect (i.e., eddy currents) across laminations and hysteresis can be resolved accurately. Such coupled models are seldom reported in the literature. With this model, material parameters for laminated structures can be identified from measurements on a rigorous theoretical basis in order to be exploited afterwards in the modeling of macroscopic devices (e.g., electrical machines) by means of a homogenization approach such as the one proposed in [4].

Practically, the proposed model consists of a 1D vector finite element (FE) modelization across half a lamination thickness. An h-field formulation is used to solve the eddy current problem, together with

*Correspondence to: S. Steentjes, Institute of Electrical Machines (IEM), RWTH Aachen University, Schinkelstr. 4, D-52056 Aachen, Germany.
†E-mail: simon.steentjes@iem.rwth-aachen.de

an implementation of the energy-based hysteresis model described in [5]. It is shown that this across-lamination model describes the metrological characteristics of non-oriented electrical steel accurately and allows an exact material parameter identification from Epstein frame (EF) or single-sheet tester measurements at any frequency.

2. THERMODYNAMIC FOUNDATION

The proposed model builds on the thermodynamic representation of the hysteresis proposed in [5–7]. It also gets some inspiration from the kinematic hardening theory of plasticity discussed in [8–10]. The first and second principles of thermodynamics are explicitly accounted for in the formulation of the model. The model relies on a mechanical anology discussed in Section 2.3.

2.1. Empty space magnetization

To appropriately account for the susceptibility of empty space, the magnetic flux density is represented as a sum

$$\boldsymbol{b} := \boldsymbol{J_0} + \boldsymbol{J} \tag{1}$$

of two components: an empty space magnetization $\boldsymbol{J}_0 := \mu_0 \boldsymbol{h}$ (where μ_0 is the magnetic permeability of vacuum), which is always linear and reversible, and a material magnetization $\boldsymbol{J}$, associated with the presence of microscopic moments attached to the atoms of the material body and that is both nonlinear and irreversible.

2.2. Energy conservation

The hysteresis model used in this paper follows directly from the expression of the conservation of energy in the material

$$\dot{\Psi} = \dot{W} + \dot{Q} \quad \Rightarrow \quad \dot{\Psi} = \boldsymbol{h} \cdot \dot{\boldsymbol{b}} - D \tag{2}$$

where Ψ stands for the energy density, $\dot{W} := \boldsymbol{h} \cdot \dot{\boldsymbol{b}}$ is the rate of magnetic work, and $\dot{Q} = -D$ is a dissipation function D. The dot above a symbol stands for a total time derivative.

The energy density is the sum of an empty space energy depending on $\boldsymbol{J}_0$ and an internal energy u depending on $\boldsymbol{J}$

$$\Psi(\boldsymbol{J}_0, \boldsymbol{J}) = \frac{\boldsymbol{J}_0^2}{2\mu_0} + u(\boldsymbol{J}) \tag{3}$$

with μ_0 as the magnetic permeability of vacuum. Its time derivative writes

$$\dot{\Psi} = \frac{\boldsymbol{J}_0}{\mu_0} \dot{\boldsymbol{J}}_0 + \boldsymbol{h}_r \cdot \dot{\boldsymbol{J}} \quad \text{with} \quad \boldsymbol{h}_r = \partial_{\boldsymbol{J}} u. \tag{4}$$

We shall call the field $\boldsymbol{h}_r$ *reversible magnetic field* because, as (4) shows, the magnetic work it delivers is integrally converted into internal energy.

2.3. Mechanical interpretation

Hysteresis losses can be interpreted as the power delivered by a constant amplitude generalized force parallel to the variation of the magnetization, that is, the magnetic equivalent of a dry friction force [5]. The physical origin of this force is the pinning effect that opposes the motion of Bloch walls.

In a thermodynamic approach, functionals are primary quantities from which constitutive relationships are derived by application of general principles. The actual characteristics of the considered

DOI: 10.1002/jnm

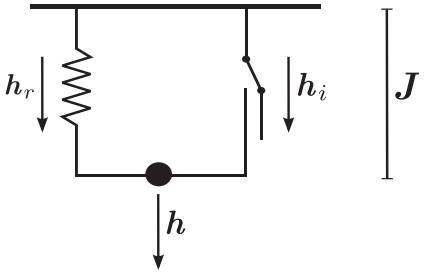

Figure 1. Mechanical analogy.

ferromagnetic material are thus introduced in the system by selecting appropriate expressions for the functionals u and D.

There exists an analogy with the stress–strain model of St Venant with hardening. Hardening is introduced by connecting nonlinear springs in parallel with a slider, that is, a friction element characterized by a limit force κ (Figure 1). The magnetic field $\boldsymbol{h}$ corresponds to the stress, whereas the magnetization $\boldsymbol{J}$ corresponds to the elongation. Starting from zero, the applied magnetic field $\boldsymbol{h}$ is increased. Before it reaches the limit κ ($\boldsymbol{h} < \kappa$), the applied field is equilibrated by the force of the slider, and no magnetization occurs ($\dot{\boldsymbol{J}} = 0$). When $\boldsymbol{h}$ reaches the limit force κ, the slider is set into motion, which means that the magnetization $\boldsymbol{J}$ increases. The power delivered in the slider $\kappa\dot{\boldsymbol{J}}$ is dissipated, whereas the recoverable energy stored in the spring increases. When the magnetic field $\boldsymbol{h}$ comes down below κ again, the slider gets locked, and magnetization is frozen ($\dot{\boldsymbol{J}} = 0$).

2.4. Dissipation

The dissipation function

$$D = \kappa|\dot{\boldsymbol{J}}| = \boldsymbol{h}_i \cdot \dot{\boldsymbol{J}} \tag{5}$$

describes hysteresis dissipation as the magnetic analogous of the work delivered by a dry friction force, whose physical origin is the pinning forces that opposes the motion of Bloch walls. We shall call the field $\boldsymbol{h}_i$ *irreversible magnetic field* because, as (5) shows, the magnetic work it delivers is integrally dissipated.

The functional (5) is not differentiable for $\dot{\boldsymbol{J}} = 0$ (so, one is not allowed to simply write $\boldsymbol{h}_i = \partial_{\dot{\boldsymbol{J}}} D$), but as it is convex, one can write

$$\boldsymbol{h}_i \in \partial_{\dot{\boldsymbol{J}}} D \tag{6}$$

where the set

$$\partial_{\dot{\boldsymbol{J}}} D = \left\{\boldsymbol{h}_i, |\boldsymbol{h}_i| \leqslant \kappa \quad \text{if } \dot{\boldsymbol{J}} = 0, \quad \boldsymbol{h}_i = \kappa \boldsymbol{e}_{\dot{\boldsymbol{J}}} \quad \text{otherwise}\right\}, \tag{7}$$

where $\boldsymbol{e}_{\boldsymbol{y}} := \boldsymbol{y}/|\boldsymbol{y}|$ denotes the unit vector parallel to the vector $\boldsymbol{y}$, is the subgradient of the functional D.

2.5. Constitutive relationships and update rule

The conservation of energy (2) now implies

$$\frac{\boldsymbol{J}_0}{\mu_0} \cdot \dot{\boldsymbol{J}}_0 + \boldsymbol{h}_r \cdot \dot{\boldsymbol{J}} = \boldsymbol{h} \cdot (\dot{\boldsymbol{J}}_0 + \dot{\boldsymbol{J}}) - \boldsymbol{h}_i \cdot \dot{\boldsymbol{J}} \tag{8}$$

and, gathering terms,

$$(\boldsymbol{h} - \boldsymbol{J}_0/\mu_0) \cdot \dot{\boldsymbol{J}}_0 + (\boldsymbol{h} - \boldsymbol{h}_r - \boldsymbol{h}_i) \cdot \dot{\boldsymbol{J}} = 0 \qquad \forall \dot{\boldsymbol{J}}_0, \dot{\boldsymbol{J}}. \tag{9}$$

DOI: 10.1002/jnm

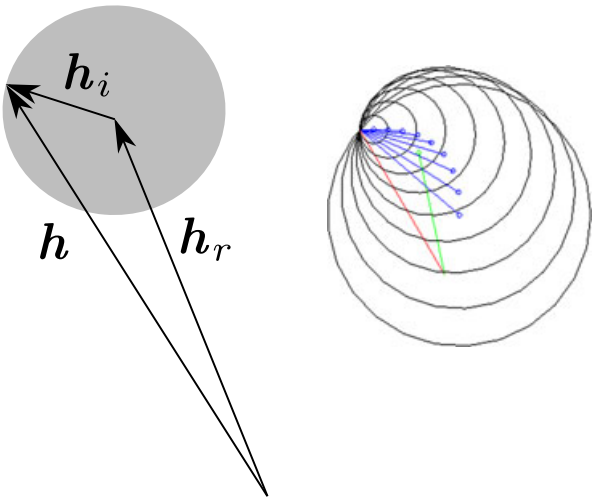

Figure 2. Left : graphical representation of the vector equation (10). The gray circle represents the subgradient (7). Right : case with n spheres.

As the state variables $\boldsymbol{J}$ and $\boldsymbol{J}_0$ are arbitrary, the factors between parenthesis must vanish, and the constitutive relationships are obtained: namely $\boldsymbol{J}_0 = \mu_0 \boldsymbol{h}$ and

$$\boldsymbol{h} - \boldsymbol{h}_r - \boldsymbol{h}_i = 0 \quad \Rightarrow \quad \boldsymbol{h} - \boldsymbol{h}_r \in \partial_{\boldsymbol{J}} D. \tag{10}$$

where we have used (4) and (6). This, at first sight, obscure equation can be given a clear pictorial representation, Figure 2 (left). The gray sphere centered at $\boldsymbol{h}_r$ is the representation of the subgradient. Starting from the situation depicted in Figure 2, if the tip of applied magnetic field $\boldsymbol{h}$ enters the sphere, the reversible magnetic component $\boldsymbol{h}_r$ is not modified. As $\boldsymbol{h}_r$ and $\boldsymbol{J}$ are in a 1-1 relationship, no change in the magnetic polarization occurs either, $\dot{\boldsymbol{J}} = 0$, and both $\boldsymbol{h}_r$ and $\boldsymbol{J}$ remain unmodified as long as the tip of $\boldsymbol{h}$ remains inside the sphere. If now the magnetic field $\boldsymbol{h}$ tends to reach out of the sphere, which is forbidden by the inclusion condition (10), the sphere must be shifted. In this case, one has $\dot{\boldsymbol{J}} \neq 0$, and (7) yields $\boldsymbol{h}_i = \kappa \dot{\boldsymbol{J}}$. Substituting in (10) gives an evolution equation for $\boldsymbol{h}_r$:

$$\boldsymbol{h} = \boldsymbol{h}_r + \kappa \boldsymbol{e}_{\dot{\boldsymbol{J}}(\boldsymbol{h}_r)} = \boldsymbol{h}_r + \boldsymbol{h}_i. \tag{11}$$

Defining the susceptibility tensor $\underline{\chi}(\boldsymbol{h}_r)$ by

$$\dot{\boldsymbol{J}}(\boldsymbol{h}_r) = (\partial_{\boldsymbol{h}_r} \boldsymbol{J}) \cdot \dot{\boldsymbol{h}}_r := \underline{\chi}(\boldsymbol{h}_r) \cdot \dot{\boldsymbol{h}}_r, \tag{12}$$

it appears that (11) is an implicit and nonlinear differential equation in $\boldsymbol{h}_r$ (h is given, and κ and $\underline{\chi}$ are known material characteristics). Its solution is rather delicate and demanding in terms of computational time, but an approximate solution can be obtained with the explicit rule, which is the implementation of the mathematical notion of subgradient arising from (7)

$$\boldsymbol{h}_r = \text{Update}(\boldsymbol{h}, \boldsymbol{h}_r^{(p)}, \kappa) := \begin{cases} \boldsymbol{h} - \kappa \frac{\boldsymbol{h} - \boldsymbol{h}_r^{(p)}}{|\boldsymbol{h} - \boldsymbol{h}_r^{(p)}|} = \boldsymbol{h} - \boldsymbol{h}_i & \text{if } |\boldsymbol{h} - \boldsymbol{h}_r^{(p)}| \geqslant \kappa \\ \boldsymbol{h}_r & \text{otherwise} \end{cases} \tag{13}$$

DOI: 10.1002/jnm

where the exponent (p) indicates a quantity evaluated at the previous time step. One has indeed

$$\begin{aligned}\boldsymbol{h}_i &= \boldsymbol{h} - \text{Update}(\boldsymbol{h}, \boldsymbol{h}_r^{(p)}, \kappa) \quad // \, \boldsymbol{h} - \boldsymbol{h}_r^{(p)} \\ \dot{\boldsymbol{h}}_r &= \frac{1}{\Delta t}\left(\text{Update}(\boldsymbol{h}, \boldsymbol{h}_r^{(p)}, \kappa) - \boldsymbol{h}_r^{(p)}\right) \\ &= \frac{1}{\Delta t}\left(1 - \frac{\kappa}{|\boldsymbol{h} - \boldsymbol{h}_r^{(p)}|}\right) \cdot (\boldsymbol{h} - \boldsymbol{h}_r^{(p)}) \quad // \, \boldsymbol{h} - \boldsymbol{h}_r^{(p)}\end{aligned}$$

where the symbol // means *is parallel to*, which shows that the simplified update rule ensures $|\boldsymbol{h}_i| = \kappa$, but $\boldsymbol{h}_i \,//\, \dot{\boldsymbol{h}}_r$ (compare the two aforementioned equations) instead of $\boldsymbol{h}_i \,//\, \dot{\boldsymbol{J}}$ as in (11). The simplified rule is thus exact in all situations where $\dot{\boldsymbol{J}} \,//\, \dot{\boldsymbol{h}}_r$, that is, in unidirectional problems (which is the case in all experimental setups), in the linear part of the magnetic curve, and in case of rotational hysteresis. In other situations, the simplified rule is an approximation.

2.6. Saturation characteristic

If the material is assumed isotropic, the vector relationship $\boldsymbol{h}_r = \partial_{\boldsymbol{J}} u(\boldsymbol{J})$ (4) yields colinear $\boldsymbol{J}$ and $\boldsymbol{h}_r$ fields; it is also one-to-one. The inverse of this function is called anhysteretic magnetization curve. Experience shows that it can be represented accurately with a parametric function

$$J(h_r) = J_a L\left(\frac{h_r}{h_a}\right) + J_b L\left(\frac{h_r}{h_b}\right) \quad , \quad \boldsymbol{J}(\boldsymbol{h}_r) = J(|\boldsymbol{h}_r|)\frac{\boldsymbol{h}_r}{|\boldsymbol{h}_r|},$$

with

$$L(x) = \coth x - \frac{1}{x}$$

the Langevin function. The four parameters of the double Langevin function $(J_a, h_a, J_b, and h_b)$ are identified from measurements as explained in Section 4.2. The Langevin function indexed with a b represents the magnetization due to the motion of Bloch walls. The second Langevin function represents the additional magnetization occurring at high field intensity that is associated with the rotation of the magnetic moments relative to the preferred axis (coherent rotation).

As the anhysteretic curve is one-to-one, it can be inverted to express $h_r(J)$ and obtain a general expression for the energy density

$$u(\boldsymbol{J}) := \int_0^{|\boldsymbol{J}|} h_r(x)\,\mathrm{d}x \quad , \quad \partial_{\boldsymbol{J}} u = h_r(|\boldsymbol{J}|)\,\boldsymbol{e}_{\boldsymbol{J}}. \tag{14}$$

Note that the Langevin function cannot be inverted analytically, but it can be inverted numerically without difficulty. A number of invertible functions have similar characteristics and present alternatives to describe the anhysteretic curve. The Langevin function has been preferred in this study because it has a statistical mechanics justification briefly explained in [5].

2.7. The model with n spheres

In the form presented so far, the model has only five parameters: four to represent the anhysteretic curve, which as we mentioned in the previous text is enough for a good accuracy, and only one, κ, to represent dissipation. Although this is already sufficient to represent the main hysteresis cycle, an accurate representation of inner cycles requires larger numbers of parameters. The accuracy of the model depends actually on a correct representation of the statistical distribution of pinning point strengths in the ferromagnetic microstructure. The characteristics of this distribution vary largely across the different types of soft and hard ferromagnetic materials and must be identified from measurements for each material.

DOI: 10.1002/jnm

The idea is to decompose the magnetization $\boldsymbol{J}$ into n fractions $\boldsymbol{J}^k$

$$\boldsymbol{J} = \sum_{k=1}^{n} \boldsymbol{J}^k \tag{15}$$

subjected to friction forces of different amplitudes κ^k so that the dissipation functional (5) now writes

$$D = \sum_{k=1}^{n} \kappa^k |\dot{J}^k|. \tag{16}$$

Let the set of scalar coefficients $\{\omega^k, k = 1, \ldots, n, \sum_{k=1}^{n} \omega^k = 1\}$ form a partition of unity. If one defines provisionally $\boldsymbol{J}^k := \omega^k \boldsymbol{J}$, that is, all $\boldsymbol{J}^k$ are assumed parallel to $\boldsymbol{J}$, the variation of internal energy (14) can be written as a sum of fraction related terms

$$\dot{u}(\boldsymbol{J}) = \left(\sum_{k=1}^{n} \omega^k \right) \boldsymbol{h}_r(J) \cdot \dot{\boldsymbol{J}} := \sum_{k=1}^{n} \boldsymbol{h}_r \left(\frac{J^k}{\omega^k} \right) \cdot \dot{\boldsymbol{J}}^k = \sum_{k=1}^{n} \dot{u}^k(\boldsymbol{J}^k) \tag{17}$$

with

$$u^k(\boldsymbol{J}^k) := \int_0^{|\boldsymbol{J}^k|} h_r \left(\frac{x}{\omega^k} \right) \mathrm{d}x \quad , \quad \boldsymbol{h}_r^k := \partial_{\boldsymbol{J}^k} u^k = h_r \left(\frac{J^k}{\omega^k} \right) \boldsymbol{e}_{\boldsymbol{J}^k} \tag{18}$$

and hence, assuming $\boldsymbol{J}^k = \omega^k \boldsymbol{J}$,

$$\boldsymbol{h}_r(\boldsymbol{J}) = \sum_{k=1}^{n} \omega^k \boldsymbol{h}_r^k \left(\frac{J^k}{\omega^k} \right). \tag{19}$$

The approach we have adopted for the model with n spheres has some similarities with a multiscale approach. *Localization* requires that each fraction could be resolved independently. For this, (18) is taken as a definition of the internal energy of the fraction k. The *homogenization* assumption, counterpart of the localization assumption, consists in assuming (19).

Gathering all elements, one obtains

$$\boldsymbol{h} - \boldsymbol{h}_r^k - \boldsymbol{h}_i^k = 0, \quad k = 1, \ldots, n. \tag{20}$$

This amounts to connect in series n hysteresis cells like the one depicted in Figure 1, with each cell having a different value of κ (Figure 3).

With n spheres, the update rule (13) is modified as follows

$$\boldsymbol{h}_r^k = \mathrm{Update}(\boldsymbol{h}, \boldsymbol{h}_r^{k(p)}, \kappa^k) := \begin{cases} \boldsymbol{h} - \kappa^k \frac{\boldsymbol{h} - \boldsymbol{h}_r^{k(p)}}{|\boldsymbol{h} - \boldsymbol{h}_r^{k(p)}|} & \text{if } |\boldsymbol{h} - \boldsymbol{h}_r^{k(p)}| \geqslant \kappa^k \\ \boldsymbol{h}_r^k & \text{otherwise} \end{cases} \tag{21}$$

the exponent $^{(p)}$ indicating a quantity evaluated at the previous time step.

The piecewise representation chosen here, with n discrete values for κ, allows a rather straightforward implementation in the FE code. As the number of divisions n can be chosen arbitrarily large, it implies no limitation on the accuracy either.

DOI: 10.1002/jnm

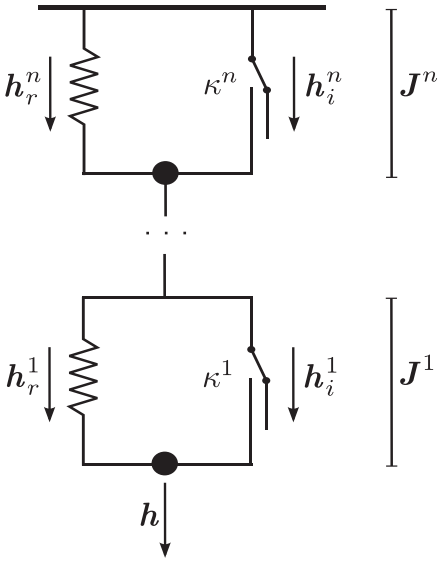

Figure 3. Pictorial representation of the model with N internal variables.

3. FINITE ELEMENT IMPLEMENTATION

3.1. 3D formulation

As the magnetic field is the natural driving quantity for the irreversible constitutive relationship (10), problems with hysteresis are naturally solved with an h-field formulation.

The weak formulation of Faraday's law reads for a set of suitable chosen test functions $\boldsymbol{h}'$ [11]:

$$\int_\Omega \left(\dot{\boldsymbol{b}} \cdot \boldsymbol{h}' + \sigma^{-1} \mathrm{curl}\, \boldsymbol{h} \cdot \mathrm{curl}\, \boldsymbol{h}'\right) d\Omega = 0 \quad \forall \boldsymbol{h}' \in \mathcal{H} \tag{22}$$

with $\mathcal{H}$ as an appropriate functional space fulfilling Dirichlet boundary conditions.

Practically, the anhysteretic curve is represented in the FE implementation as a curve giving the magnetic susceptibility $\chi := J/h_r$ as a function of $|\boldsymbol{h}_r|^2$, with $\boldsymbol{h}_r$ defined by (19). The magnetic flux density (1) is then

$$\boldsymbol{b}(\boldsymbol{h}, \boldsymbol{h}_r) = \mu_0 \boldsymbol{h} + \chi(|\boldsymbol{h}_r|^2)\, \boldsymbol{h}_r, \tag{23}$$

and its time derivative in terms of the unknown $\boldsymbol{h}$ writes (note the dyadic product $\boldsymbol{h}_r \boldsymbol{h}_r$)

$$\dot{\boldsymbol{b}}(\boldsymbol{h}, \boldsymbol{h}_r) = \left(\mu_0 + \left(\chi(|\boldsymbol{h}_r|^2)\mathbb{I} + 2\dot{\chi}(|\boldsymbol{h}_r|^2)\, \boldsymbol{h}_r \boldsymbol{h}_r\right) \partial_{\boldsymbol{h}} \boldsymbol{h}_r\right) \dot{\boldsymbol{h}} := \underline{\mu}^{\partial} \cdot \dot{\boldsymbol{h}} \tag{24}$$

where $\mathbb{I}$ is the identity matrix. The tangent permeability tensor $\underline{\mu}^{\partial}$ is expressed in terms of $\partial_{\boldsymbol{h}} \boldsymbol{h}_r$, which is expressed in terms of fraction quantities by a formal derivation of the update rule (21)

$$\partial_{\boldsymbol{h}} \boldsymbol{h}_r = \sum_{k=1}^{n} \omega^k \partial_{\boldsymbol{h}} \boldsymbol{h}_r^k = \sum_{k=1}^{n} \omega^k\, \partial_{\boldsymbol{h}} \mathrm{Update}(\boldsymbol{h}, \boldsymbol{h}_r^{k(p)}, \kappa^k). \tag{25}$$

The FE resolution proceeds by time stepping over a few periods of the applied magnetic field. At each new time step, the $\boldsymbol{h}_r^k$'s are updated according to the new value of the applied magnetic field $\boldsymbol{h}$ following the rule (21).

DOI: 10.1002/jnm

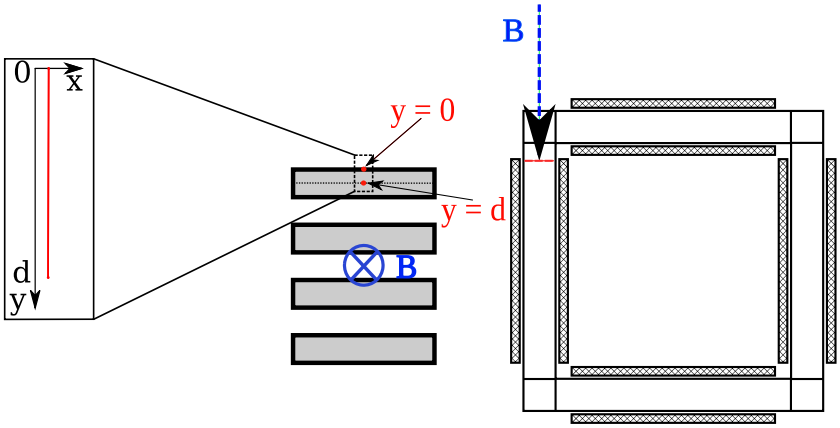

Figure 4. Finite element domain of study.

3.2. 1D formulation

The measured quantities in EFs or single-sheet testers experiments are currents and fluxes related to the magnetic field $\boldsymbol{h}_0$ at the surface of the lamination and the average magnetic flux density $\langle \boldsymbol{b} \rangle$ across the lamination thickness, respectively. Accounting for the symmetries of the measurement tools, it is thus sufficient to work with an FE model that consists of a 1D formulation of the eddy current problem with $\boldsymbol{h} = (0, h(z), 0)$. Considering a lamination of thickness $2d$ with an upper surface normal vector $\boldsymbol{n} = (0, 0, 1)$, the domain of analysis Ω is a line parallel to $\boldsymbol{n}$, across half the thickness, and far from the edges (Figure 4). The boundary condition at the center of the lamination is $\text{curl}\, \boldsymbol{h}(0) \times \boldsymbol{n} = 0$, whereas a given external field $\boldsymbol{h}(d)$ is applied at the surface of the lamination. Iron losses per unit surface are given by the flux of the Poynting vector $\sigma^{-1}\text{curl}\, \boldsymbol{h}(d) \times \boldsymbol{h}(d)$ across the lamination surface.

4. MATERIAL PARAMETERS

4.1. Metrological characterization

The material under study, referenced as *M235-35A*, is a non-grain-oriented FeSi 3.2% steel lamination of thickness of 0.35 mm. The measurements are done under standardized EF protocols. EFs (Figure 5) are measurement apparatus utilizing the field-metric method under sinusoidal magnetic flux densities. They are equipped with different numbers of primary and secondary windings for different frequency ranges. Quasi-static material characteristics, on the other hand, are identified by point-by-point DC-measurements using a flux meter. The covered magnetic flux density range is 0.1–1.5 T.

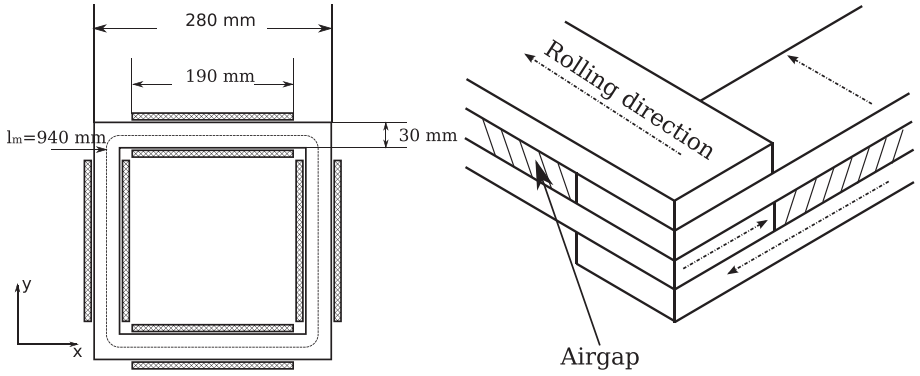

Figure 5. Left : overall dimensions of the Epstein frames. Right : sample arrangement in different layers.

DOI: 10.1002/jnm

The EF used in this study has 24 stripes (of dimension 280 mm x 30 mm, Figure 5 left). The stripes are arranged so as to compensate the anisotropy due to the rolling direction. In one layer, the stripes are arranged alternately in accordance with the rolling direction, that is, a sample in the rolling direction is followed by a sample perpendicular to the rolling direction. In the layer immediately below, the sample arrangement is shifted by 90 degrees (Figure 5 right). Measurements are carried out at various frequencies, ranging from quasi-static to 700 Hz.

4.2. Identification strategy

Working with n fractions, the hysteresis model has $2n + 4$ parameters to identify: the four free parameters of the double Langevin function (2.6.) and the $2n$ fraction related parameters κ^k and ω^k. Because the measured data is unidirectional, it is sufficient to work with scalar values. Parameter identification is done in two steps.

The parameters describing the local pinning forces κ^k ($\kappa^1 < ... < \kappa^n$) and their weighting parameters ω^k are first determined on the basis of the coercive field versus maximum magnetic field characteristic. This $h_c(h_{max})$ characteristic is obtained from the measurement of a series of hysteresis loop of increasing amplitudes h_{max} and then identified with the parametrized staircase function

$$\bar{h}_c(h_{max}) = \sum_{k=1}^{m(h_{max})} \omega^k \kappa^k \tag{26}$$

where $m(h_{max})$ is the higher fraction index k for which $\kappa^k < h_{max}$, that is, $\kappa^k > h_{max}, \forall k > m(h_{max})$. The identification is done by least-square fitting with the Levenberg–Marquardt algorithm. As the cost functions need continuous differentiable functions to minimize, a modified heaviside function is used having a finite gradient at the steps. The identified staircase function, with $n = 6$ fractions is shown in Figure 6.

The four parameters of the double Langevin function (2.6.) are identified on the basis of the first magnetization curve. Comparing the modeled first magnetization curve with the measured one for increasing values of the applied field $\boldsymbol{h}$, the parameters describing the double Langevin function can be identified readily.

In order to validate the identified κ^k and ω^k parameters, the response of the model in terms of hysteris loops and iron losses is compared with the available measurements. Figure 7 (left) shows quasi-static hysteresis loops obtained by feeding the model directly with the Epstein-measured magnetic field $h(t)$. Figure 7 (right) shows the match of the first magnetization curves and Figure 8

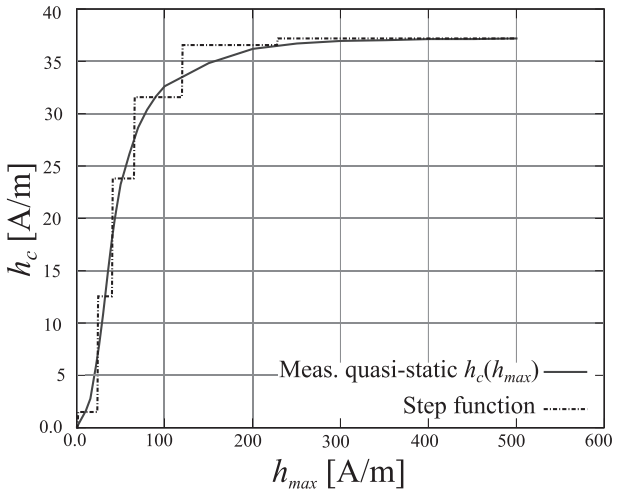

Figure 6. Coercive field h_c as a function of the applied field amplitude h_{max}. Measurement (solid line) and approximation (dotted line).

DOI: 10.1002/jnm

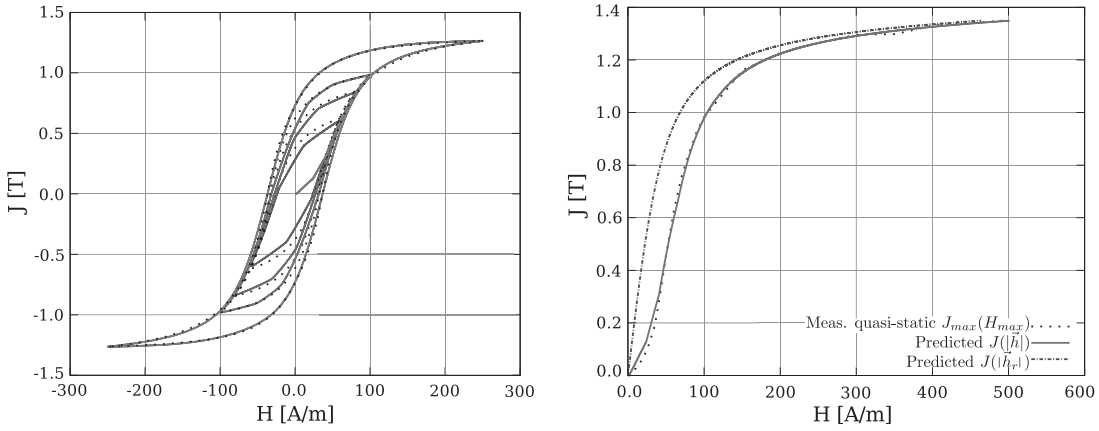

Figure 7. Left : quasi-static hysteresis loops, measured (*dotted lines*) and modeled (*solid lines*). Right : first magnetization curve, measured (*dotted lines*) and modeled (*solid line*).

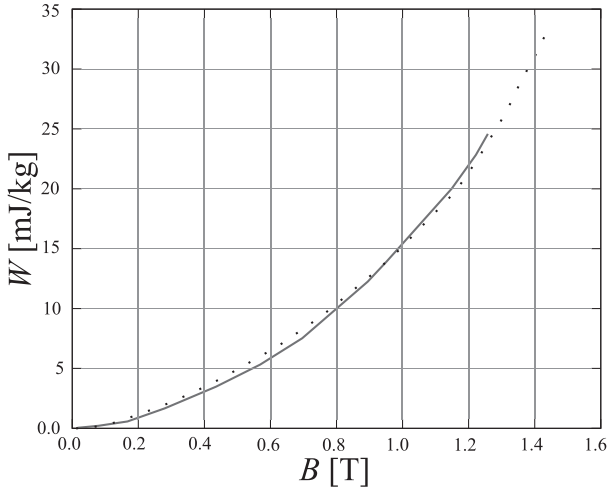

Figure 8. Quasi-static iron losses (hysteresis losses), measured (*dotted line*) and calculated (*solid line*).

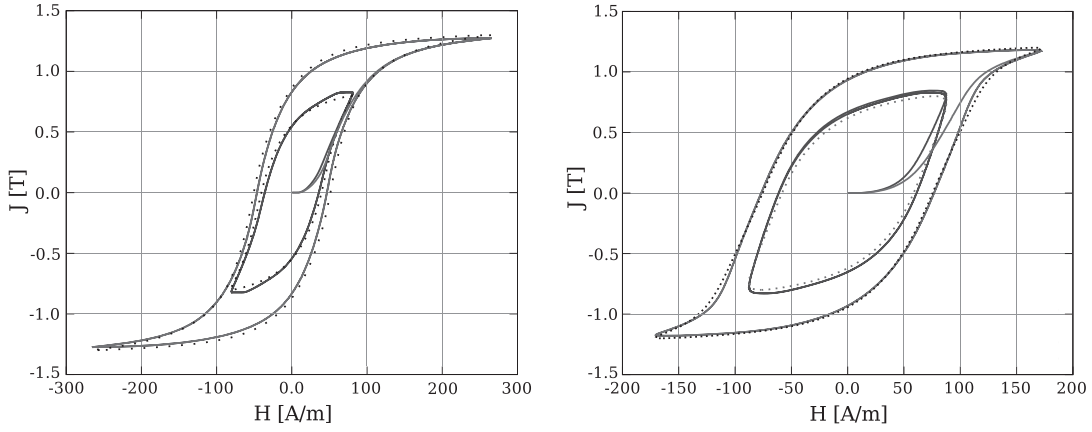

Figure 9. Hysteresis loops at higher frequencies, measured (*dotted line*) and calculated (*solid line*). Left : 50 Hz. Right : 200 Hz.

DOI: 10.1002/jnm

the match of iron loss curves. In all cases, the model shows its ability to reproduce the quasi-static measurements with an excellent accuracy.

In order to analyze the ability to reproduce dynamic hysteresis loops, hysteresis loops at 50 Hz (Figure 9 (left)) and 200 Hz (Figure 9 (right)) are compared. The proposed hysteresis model describes the bulging of the hysteresis loops quite accurately.

5. CONCLUSION

The motivation for this work is the development of constitutive models for the hysteresis phenomena. The proposed model, on the basis of the thermodynamic principles, is energy-consistent. A variational approach provides a robust and coherent framework to efficiently handle the strong nonlinearity of the problem within an FE scheme. A practical explicit update rule exists that is exact in most situations and in particular in the unidirectional case. Besides mathematical and physical elegance, this model has practical advantages. Unlike the model of Preisach and Jiles–Atherton, it is readily vectorial, and the number of parameters is not limited. Moreover, it relies on an energy balance of which the stored magnetic energy and dissipated energy are known at all times.

With this approach, hysteresis losses, accounting for vector effects (rotating hysteresis) and the presence of higher harmonics, can be evaluated with controllable accuracy. This opens up the possibility of accurate evaluations of magnetic losses in real-life electrical engineering devices: from the prediction of iron losses in electrical engineering devices (rotating machines, actuators, and brakes) to the accurate modeling of hysteresis in magnetostrictive actuators and smart materials.

The hysteresis model proposed in this paper represents a significant improvement with respect to conventional post-processing techniques based on measured loss characteristics. Because it relies on a physical assumption that it is vectorial and dynamic from the beginning (the analogy with a dry friction force), the identified parameters represent the material in general and not under specific experimental conditions. In other words, although the identification was done with experimental data assuming a sinusoidal in time and unidirectional $\boldsymbol{b}$ field, the identified parameters can be used in 2D and 3D and in the presence of higher harmonics. Another further improvement will be to deal with laminated structures explicitly by means of appropriate multi-scale techniques.

ACKNOWLEDGMENTS

The work of S. Steentjes was granted by the Deutsche Forschungsgemeinschaft (DFG) carried out in the research project ‘Improved modeling and characterisation of ferromagnetic materials and their losses’. The work of F. Henrotte was supported by the Belgian Science Policy (IAP P7/02), Belgian French Community (ARC 09/14-02), and Walloon Region (WIST3 project ‘FEDO’).

REFERENCES

1. Bertotti G. *Hysteresis in Magnetism*. Academic Press: San Diego, 1998.
2. Mayergoyz I. *Mathematical Models of Hysteresis and their Applications*, Second Edition. Academic Press: New York, 2003.
3. Jiles DC, Atherton DL. Theory of ferromagnetic hysteresis. *Journal of Magnetism and Magnetic Materials* 1986; **61**:48–60.
4. Niyonzima I, Sabariego RV, Dular P, Henrotte F, Geuzaine C. Computational homogenization for laminated ferromagnetic cores in magnetodynamics. *IEEE Transactions on Magnetics* 2013; **49**:2049–2052.
5. Henrotte F, Nicolet A, Hameyer K. An energy-based vector hysteresis model for ferromagnetic materials. *COMPEL* 2006; **25**:71–80.
6. Bergqvist A. Magnetic vector hysteresis model with dry friction-like pinning. *Physica B* 1997; **233**:342–347.
7. Henrotte F, Hameyer K. A dynamical vector hysteresis model based on an energy approach. *IEEE Transactions on Magnetics* 2006; **42**:899–902.
8. Puzrin AM, Houlsby GT. Fundamentals of kinematic hardening hyperplasticity. *Journal of Solids and Structures* 2001; **38**: 3771–3794.
9. Puzrin AM, Houlsby GT. A thermomechanical framework for constitutive models for rate-independent dissipative materials. *Journal of Plasticity* 2001; **16**:1017–1047.
10. Ortiz M, Stainier L. The variational formulation of viscoplastic constitutive updates. *Computer Methods in Applied Mechanics and Engineering* 1999; **171**: 419–444.
11. Ida N, Bastos JPA. *Electromagnetics and Calculation of Fields*. Springer: New York, 1992.

DOI: 10.1002/jnm